Macromolecular Rapid Communications
www.mrc-journal.de

Mesoporous Silica Micromotors with a Reversible Temperature Regulated On–Off Polyphosphazene Switch

*Michael Kneidinger, Aitziber Iturmendi, Christoph Ulbricht, Tia Truglas, Heiko Groiss, Ian Teasdale, and Yolanda Salinas**

The incorporation of an extraneous on–off braking system is necessary for the effective motion control of the next generation of micrometer-sized motors. Here, the design and synthesis of micromotors is reported based on mesoporous silica particles containing bipyridine groups, introduced by cocondensation, for entrapping catalytic cobalt(II) ions within the mesochannels, and functionalized on the surface with silane-derived temperature responsive bottle-brush polyphosphazene. Switching the polymers in a narrow temperature window of 25–30 °C between the swollen and collapsed state, allows the access for the fuel H_2O_2 contained in the dispersion medium to cobalt(II) bipyridinato catalyst sites. The decomposition of hydrogen peroxide is monitored by optical microscopy, and effectively operated by reversibly closing or opening the pores by the grafted gate-like polyphosphazene, to control on demand the oxygen bubble generation. This design represents one of the few examples using temperature as a trigger for the reversible on–off external switching of mesoporous silica micromotors.

The last decades of improvements in materials science and nanotechnology have led to the design of powerful self-propelled micro- and nanomotors. These systems are capable of motion in different fluids, by utilizing either a physical energy source, such as light or ultrasound,[1] or chemical fuel, such as hydrogen peroxide, water, or acid.[2] Precise movement manipulations, like the control over the velocity and the direction, are still limited but particularly desirable.[3] Recent methods to affect the motion of micrometer-sized motors on demand have been based on the decomposition of the whole microsystem through temperature or the chemical inhibition of the catalytic activity.[4] In most of the systems, the bubble propulsion controls the velocity of the motors and depends on the concentration of fuel. Therefore, the next step in the motion-regulation evolution is the incorporation of external stimuli-responsive start/stop controls to easily regulate the movement.

Nowadays many intelligent gate-like materials responding to stimuli, such as temperature,[5] pH,[6] redox,[7] light,[8] or even biomolecules[9] have been developed. Thermoresponsive polymers are tested in various fields like targeted drug delivery and biomedical engineering,[10] sensing,[11] or catalysis[12] applications. Temperature was also the stimulus of choice in the work reported in 2017 by Wilson et al.,[13] where bowl-shaped polymeric vesicles entrapping platinum nanoparticles to catalyze oxygen formation from hydrogen peroxide were developed. There, the addition of a valve system based on poly(*N*-isopropylacrylamide) (PNIPAM) brushes with lower critical solution temperature (LCST) characteristics allowed to regulate the velocity-defining bubble formation rate by controlling catalyst and fuel interactions via the temperature settings.

The LCST transition from dissolved to collapsed state for PNIPAM and other (co)polymers is related to their intrinsic amphiphilicity, which is affected by monomer composition and molecular weight.[14] The other critical component is the employed protic solvent or solvent mixtures, most commonly water, and possible additives impacting the hydrogen bond formation between solvent and polymeric solute. Polyphosphazenes are polymers possessing a backbone formed by alternating phosphorus and nitrogen atoms. They feature high flexibility, high thermal stability, and hydrolytic degradability,[15] and can be used to prepare stimuli-responsive materials.[16] Molecular brush-type polyphosphazenes with different side chains, such as *N*-isopropylacrylamide[17] as well as a combination of hydrophilic poly(ethylene oxide) (PEO) oligomers[18] have been reported to exhibit thermoresponsive behavior.

M. Kneidinger, Dr. A. Iturmendi, Dr. C. Ulbricht, Prof. I. Teasdale, Dr. Y. Salinas
Institute of Polymer Chemistry (ICP)
Johannes Kepler University Linz
Altenberger Straße 69, 4040 Linz, Austria
E-mail: yolanda.salinas@jku.at
Dr. C. Ulbricht
Institute of Physical Chemistry-Linz Institute for Organic Solar Cells (LIOS)
Johannes Kepler University Linz
Altenberger Straße 69, 4040 Linz Austria
T. Truglas, Dr. H. Groiss
Christian Doppler Laboratory for Nanoscale Phase Transformations
Center of Surface and Nanoanalytics
Johannes Kepler University Linz
Altenberger Straße 69, 4040 Linz, Austria
The ORCID identification number(s) for the author(s) of this article can be found under https://doi.org/10.1002/marc.201900328.

DOI: 10.1002/marc.201900328

Particularly, Jeffamines are an interesting commercially available series of amine-capped statistical ethylene oxide/propylene oxide copolymers (PEO/PPO). They exhibit LCST behavior which varies depending on the comonomer ratio. In previous works, Jeffamines (namely M-1000, 2005 and 2070) were grafted to the polyphosphazene backbone to form temperature sensitive materials for drug delivery.[19]

Besides polymeric systems or metal–organic frameworks,[20] micro- or nanomotors can be prepared on the basis of mesoporous hybrid organo-silica materials. Functionalized MCM-41 or SBA-15 mesoporous type materials have been investigated for more than two decades.[21] They present a synergetic combination of organic species, silicate, and mesopores, surpassing the capabilities of conventional pure Si—O-based materials. Despite their uniform morphology and size, adaptable composition, high-dense parallel unconnected porosity, exceptional chemical stability and high surface area, their potential use as micromotors is not well explored, so far.[22] Furthermore, a facile chemical modification of the inner and outer silica surface with a wide range of organosilane derivatives is possible. In fact, mesoporous silica particles with a vast variety of covalently linked catalytic centers alongside grafted inorganic pore-blockers or with organic molecular gates (e.g., responsive polymers) have been reported.[23] Therefore, the combination of these features make these mesoporous silica scaffolds outstanding candidates for engineering advanced responsive micromotors. Herein, we report a new micromotor based on mesoporous silica microparticles containing bipyridine groups introduced by the co-condensation method. These groups act as efficient ligands for entrapping catalytic cobalt(II) ions within the mesochannels. The surface of the microparticles was functionalized with silane-derived thermoresponsive polyphosphazene brushes containing Jeffamine M-2005 moieties, which served as opening/closing switches for the control of oxygen generation due to the decomposition of hydrogen peroxide as fuel. This designed micromotor system senses mild temperature changes, leading to bubble formation and non-directional motion. The interaction of the mesoporous microparticles with hydrogen peroxide was studied by optical microscopy at different temperatures to confirm the reversible on–off switching mechanism. Our system represents one of the very few examples containing reversible temperature-triggered gates for micromotors, which advantageously do not affect the catalytic center or the particle size.

Silica mesoporous microparticles (type MCM-41) were selected for the micromotor preparation (**Figure 1**). First, their unique tube-like pores inner and outer surface was formed together with bipyridine molecules containing silane groups (SiBPy) (see experimental details in the Supporting Information). These suitable ligands were anchored within the mesopores of the silica framework by co-condensation method.[24] Predominantly, there are two types of materials according to the type of functional organic groups in the walls: using 100% of one or more bis- or multi-bridged organosilica precursors (formation of so-called periodic mesoporous organosilicas [PMO], with absence of additional silica source), or organo-bridged mesoporous silica nanomaterials (MSNs), which use less bridged organic groups together with the addition of a classical silica precursor (e.g. tetraethyl orthosilicate [TEOS] or tetramethyl orthosilicate [TMOS]).[25] Besides the advantages of preparing silica-based particles incorporating organic functionalities, in some occasions the use of complex organic groups may disturb the periodic and uniform mesostructured order. We chose the second one involving co-condensation of organosilanes together with TEOS to address that issue of maintaining the structural control. This approach ensured a homogenous distribution of the functional groups within the material, since the hydrophobic nature of the bypiridine structure promotes its incorporation into the surfactant micelles core during the silica mesoporous microparticles synthesis. For this purpose, the bipyridine ligands (SiBPy) were reacted together with the main silica source, tetraethyl orthosilicate (TEOS), and the pore-directing agent, the surfactant cetyltrimethylammonium bromide (CTAB), all in "one-pot" under basic conditions to form bipyridine-bridged mesoporous microparticles (MP-SiBPy).[26] A uniform distribution of bipyridine groups within the silica scaffold is expected to favor the later cobalt metal fixation by the regular distribution of ligands within the pores of the material.[26] In most of the reported systems, Pt metal has been widely used as catalyst,[27] though here we selected cobalt as a potential low-cost alternative in our design of micromotors. The cobalt bipyridine complex formation within the pores of the microparticles MP-SiBPy was carried out as reported in literature, yielding the material MP-SiBPy-Co.[28] The coordination between the anchored ligand sites (SiBPy) and cobalt acetate was formed under reflux in toluene. Cobalt bipyridine complexes were chosen to act as active centers placed in the pore voids, since cobalt (II) has the well-known capability to catalyze the rapid degradation of hydrogen peroxide to oxygen and water.[29]

The bubble formation control is one of the given limitations in nowadays motor design. To obtain tunable functional materials, a thermoresponsive polyphosphazene was covalently grafted onto the surface of the silica microparticles (Figure 1). The use of a bottle-brush polyphosphazene is intended to provide a dense coating for effective sealing when the polymer adopts the globule hydrated and extended conformation below LCST, closing the pores. Upon external temperature operation changes, the bubble formation is regulated by opening the pores through the random coil conformation adopted by the polymer above its LCST (switched on MP-SiBPy-Co-PPz4 micromotor). Same mechanism was observed by Lopez et al.[5] who described a system based on PNIPAM as temperature-responsive cap. In our case, the lower critical solution temperature (LCST) of such a polymer can be easily adjusted according to the selected substituents.[19] Here, polyphosphazenes containing Jeffamine M-2005 moieties to bring thermoresponsiveness and alkoxysilane groups, to facilitate its thermoresponsiveness, and akoxysilane groups, to facilitate its attachment onto the silica suface of the microparticles, were prepared. To the best of our knowledge, this kind of polymer was never before utilized as a responsive molecular-gate-like functionality on mesoporous silica materials.

In the first step of the micromotor preparation, bipyridine ligands equipped with four organosilane-functionalities (SiBPy) were anchored through covalent —Si—O—Si—bonds within the walls of the mesochannels during co-condensation with TEOS yielding functional MPSiBBy microparticles. To obtain this trimethoxysilane ligand (SiBPy), thiol-yne addition[30] of 3-mercaptopropyl trimethoxysilane was used to link the triple bonds of the prepared bipyridine derivative BPy-alkyne (for

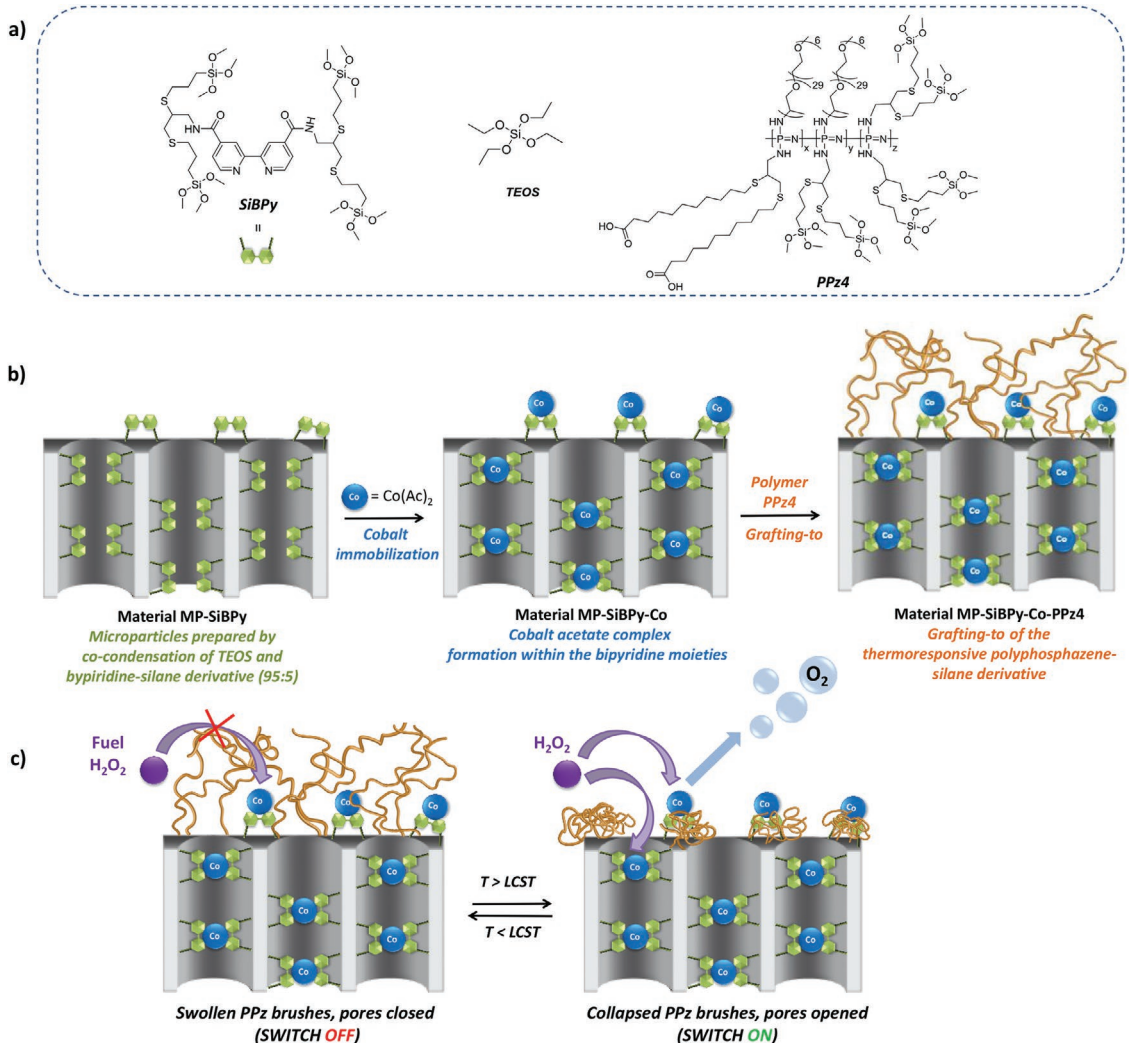

Figure 1. Schematic design of silica-based micromotors with thermoresponsive polymeric switches: a) chemical structures of functional bipyridine moieties containing alkoxysilanes (SiBPy), TEOS, and thermoresponsive polyphosphazene PPz4. The scheme of the polymer shows combinations of the three different substituents statistically distributed along the backbone in a ratio of approximately 2:1:3 (Jeffamine M-2005:11-mercaptoundecanoic acid moieties:alkoxysilane groups). b) Preparation of silica-based micromotors (MP-SiBPy-Co-PPz4) by using TEOS:SiBPy (95:5) via co-condensation, followed by cobalt immobilization forming SiBPy-Co complexes, and finally polymer PPz4 grafting-to the silica surface. This scheme represents a small section of a whole microparticle where the polymer is covering all around the silica outer surface. c) Reversible behavior of the polyphosphazene PPz4 by increasing the temperature above LCST, which lets hydrogen peroxide (fuel) access the catalytic cobalt sites forming oxygen bubbles (micromotor switched on).

experimental details see Supporting Information). Afterward, a mixture of TEOS and the corresponding synthetized silane-derived bipyridine (SiBPy) in molar ratio 95:5 was used. The ratio was selected to avoid any significant morphological changes, but still incorporate sufficient ligands to construct the heterogeneous catalysis system. The reagents molar ratio was fixed to 2.9:1:0.26:0.3 for TEA/silica source (TEOS:SiBPy, 95:5)/CTAB/NaOH similarly as in our previous work.[31] Because of the presence of organic content within the pores, the surfactant was removed by ammonium nitrate extraction method[31] in ethanol instead of common calcination. The organic moieties were fixed within the siloxane framework as described by Kapoor et al.[26] and the SiBPy-functionalized microparticles were called MP-SiBPy. Porous non-functionalized microparticles (type MCM-41) were synthesized via the "atrane route" described in literature[32] using 100% of common silica source TEOS (so-called MP-nf after surfactant removal), and used as a control material.

The prepared microparticles MP-SiBPy were characterized by nitrogen adsorption–desorption analysis (Figure S9a, Supporting Information) and compared to the control material (MP-nf) which presented non-functional moieties. The MP-SiBPy microparticles showed smaller pore volume and surface area (0.75 $cm^3\ g^{-1}$ and 697 $m^2\ g^{-1}$, respectively, shown in **Table 1**) than the control material MP-nf, which showed expected features typical of MCM-41-type mesoporous silica (pore volume of ≈0.9 $cm^3\ g^{-1}$, surface area of ≈1100 $m^2\ g^{-1}$, and pore size of 2.6 nm, see Table 1),[33] indicating the successful ligand functionalization. In this case, slightly larger pore sizes of 3.9 nm were obtained (see Figure S9c, Supporting Information). The general morphology of MP-SiBPy was not affected by the co-condensation method,

Table 1. Characterization parameters from the prepared materials MP-nf, MP-SiBPy, MP-SiBPy-Co, and MP-SiBPy-Co-PPz4 by N_2-adsorption–desorption isotherms and by dynamic light scattering.

Material	S_{BET} area[a)] [$m^2\ g^{-1}$]	Pore volume[a)] [$cm^3\ g^{-1}$]	Pore size[a)] [nm]	dH number[b)] [nm]	Zeta potential[b)] [mV]
MP-nf	1102	0.88	2.6	545 ± 80	−43 ± 5
MP-SiBPy	697	0.75	3.9	660 ± 133	−42 ± 9
MP-SiBPy-Co	484	0.55	4.1	674 ± 59	−19 ± 4
MP-SiBPy-Co-PPz4	469	0.52	—	771 ± 144	−29 ± 6

[a)]Surface area determined by applying BET model. Pore volumes and sizes were estimated by BJH model; [b)]Hydrodynamic diameters and Zeta potential obtained by DLS (average values from at least three independent measurements).

as seen in TEM images (see **Figure 2**a), and the microparticles features were considered to be sufficient for the envisioned cobalt catalyzed reaction through the immobilized cobalt and mass transfer from the mesochannels.

The content of SiBPy was analyzed by thermogravimetric analysis (TGA, shown in Figure S8b, Supporting Information) and 0.67 mmol of BPy moieties per gram of silica was calculated. Based on this value, cobalt acetate was added in excess to prepare the catalytic active particles MP-SiBPy-Co. After purification, a metal loading of ≈6 wt% was obtained, which was in accordance with other metal loadings reported for bipyridine-functionalized MCM-41 materials by Nunes and coworkers.[34] The pore volume and the surface area of the material MP-SiBPy after coordination of cobalt acetate to the bipyridine units was reduced from 0.75 to 0.55 $cm^3\ g^{-1}$, and from 697 to 484 $m^2\ g^{-1}$, with no significant pore size changes. This was a good indication that the Co-bipyridine complex may have occurred mostly in the inner pores, as reported for similar mesoporous organosilica systems.[35] In order to further validate that assumption, the presence and position of cobalt in MP-SiBPy-Co was clearly verified by STEM-EDX mapping measurements of a region with well-resolved pores in

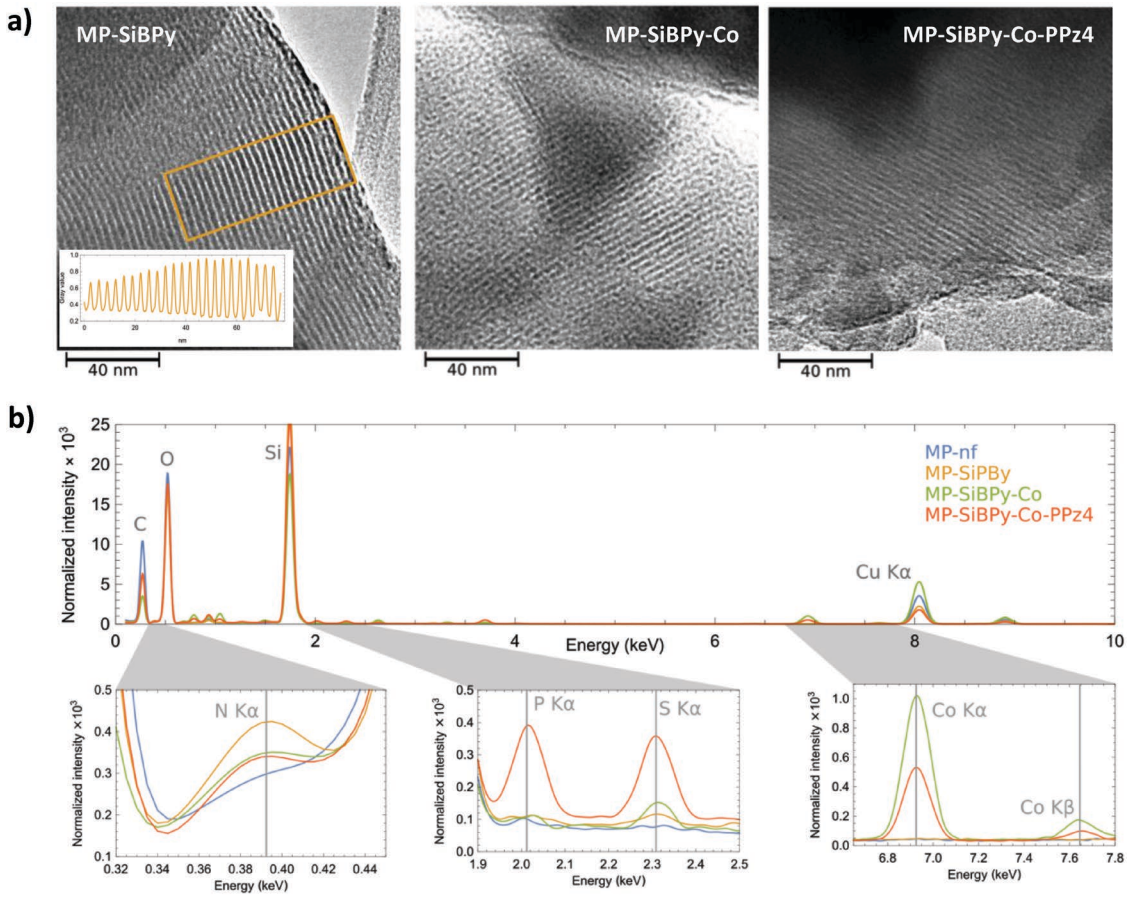

Figure 2. a) High-resolution TEM images of the mesoporous microparticles, deposited on copper TEM-grids, showing an odered, longitudinal porosity for MP-SiBPy, MP-SiBPy-Co, and MP-SiBPy-Co-PPz4, from left to right, respectively. Scale bar: 40 nm. The TEM image intensity normal to the pore direction was extracted to determine the pore size, as shown in MP-SiBPy inset (left image). The resulting line profiles yielded a typical pore size of 3–4 nm. b) Lowpass-filtered STEM EDX spectra of MP-nf, MP-SiBPy, MP-SiBPy-Co, and MP-SiBPy-Co-PPz4. Insets show zoomed-in spectral regions for the elements N, P, S, and Co.

material MP-SiBPy-Co (Figure S12, Supporting Information) where the elements O, Si, N, S, and Co were detected. Cobalt was observed to be mainly located within the silica mesopores, resulted from the immobilization of Co ions with SiBPy ligands by complex formation.

For the last step, thermoresponsive bottle-brush polyphosphazenes were prepared, containing three different substituents in different ratios: 34% Jeffamine M-2005, 18% 11-mercaptoundecanoic acid moieties, and 48% 3-mercaptopropyl trimethoxysilane groups, where % stands for estimated phosphorus atoms functionalized per repeating unit. The final polymer (so-called PPz4) was the result of four reaction steps. At first, phosphine-mediated living polymerization of $Cl_3P{=}N{-}SiMe_3$ was carried out according to similar reported procedure[26] (experimental details in Supporting Information) yielding the precursor poly(dichloro)phosphazene $[NPCl_2]_n$ with an estimated 50 repeating units (^{31}P NMR, see Figure S2, Supporting Information). This starting polymer (referred as PPz1) was substituted with propargylamine followed by Jeffamine M-2005 in the ratio 2:1. The derivatization of polymer backbone with grafted molecular brushes of various amino capped statistical poly-(ethylene oxide-co-propylene oxides) (PEO-PPO-NH_2), such as commercially available Jeffamines M-1000, M-2005, or M-2070, have been already reported by our group and their tuned LCST studied in detail.[36] Propargylamine was used to introduce alkyne moieties for subsequent functionalization. The second polyphosphazene (PPz2) was characterized by ^{1}H and ^{31}P NMR spectroscopy (see Figures S4 and S5, Supporting Information). The third step was the preparation of PPz3, whereby 11-mercaptoundecanoic acid was reacted by a photoinduced thiol-yne addition reaction[30] to lower the LCST values of the resultant materials, which were measured to be ≈35 °C for PPz2, however, for PPz3 a visible clouding was observed 10 °C lower, ≈25 °C (Figure S7, Supporting Information). Finally, for adding the required alkoxysilane groups that will permit the grafting of the polymer onto the silanols of the silica particles surface, the last step consisted of the reaction of 3-mercaptopropyl trimethoxysilane with the remaining propargylamine groups onto the polyphosphazene, also via thiol-yne addition to give a trimethoxysilane-functionalized polymer, so-called PPz4. Following, polymer PPz4 was grafted-to the material MP-SiBPy-Co by dispersing in ethanol under inert conditions to avoid alkoxysilanes hydrolysis, which led to the final microparticles. This material MP-SiBPy-Co-PPz4 was obtained with slightly smaller surface area and pore volume (469 $m^2\ g^{-1}$ and 0.52 $cm^3\ g^{-1}$, respectively), as expected after functionalization with the polymer (Table 1, and Figure S9a–c, Supporting Information). The content of the polymer was determined by thermogravimetry analysis as 1 wt% (Figure S9b, Supporting Information), which was enough to prevent the access of the fuel, hydrogen peroxide, at swollen state below LCST by adopting a hydrated and extended conformation closing the pores.

Scanning and transmission electron microscopy were used to determine the textural features of all the microparticles. At all three stages of the micromotor preparation, the samples exhibited longitudinal pores. In order to confirm the pore size by TEM images, the intensity orthogonal to the pore direction was extracted. The periodicity of the resulting line profile yielded a typical pore size of around 3–4 nm (inset in Figure 2a for MP-SiBPy, and Figure S10, Supporting Information for MP-nf), similar to the values obtained by nitrogen adsorption–desorption analysis (Table 1 and Figure S9a, Supporting Information). TEM and SEM images (Figures 2a and 3a) showed that the morphology of the microparticles and their pore sizes did not change significantly after each synthesis step. Thus, no changes in morphology are expected after polymer attaching, considering that the polymer layer should be in the range of 14 nm below LCST, as measured by DLS (the PPz3 hydrodynamic diameter is shown in Figure S7a, Supporting Information).

SEM investigations showed that the microparticles were irregularly shaped and images of all four samples showed the presence of individual microparticles (<500 nm in diameter), which tend to form large clusters up to several microns (**Figure 3**a). The hydrodynamic diameter (d_H) of the microparticles (from 545 to 771 nm) was moreover estimated by dynamic light scattering (DLS) measurements (see Table 1), and the results were in agreement with SEM images.

Additionally, FT-IR spectra were measured for all four materials (MP-nf, MP-SiBPy, MP-SiBPy-Co, and MP-SiBPy-Co-PPz4) showing typical absorption peaks attributed to the presence of SiBPy ligands and polymer PPz4 (Figure S11, Supporting Information). The formation of Si—O—Si network was observed in all the materials, assigned to a broad peak between at 1230 and 1036 cm^{-1}. The presence of the SiBPy ligand in the materials was determined by *ν*CCN vibrations at 1630 cm^{-1} from the pyridine groups and C=O vibrations at 1708 cm^{-1} characteristic from the amide formation. After grafting the PPz4, the peak at 1418 cm^{-1} and 1554 cm^{-1} were assigned to the polyphosphazene polymer, and further an obvious absorption band at 660 cm^{-1} was observed attributed to the −S− group, indicative of the full conversion thiol-yne addition reaction. The significant decreasing intensity of the silanols groups (Si—OH) at 970–950 cm^{-1} suggested the effective covalent attachment of the polymer on the microparticles MP-SiBPy-Co-PPz4.

To determine the composition of the microparticles, STEM-EDX was used. Figure 2b shows low-pass filtered STEM-EDX spectra from microparticles samples taken after each preparation step. The spectra were normalized with respect to the integrated counts without the elastic peak, and they were recorded preferably at locations where no underlying carbon film was present. Since the specimen thicknesses at the measured spots varied, the peak heights depicted should be interpreted qualitatively. The presence of carbon, oxygen, and silicon from the microparticles was readily visible. For the remaining light elements (N, P, and S), interpretation of the spectra was difficult due to the small concentrations, overlap with high intensity peaks (in case of N), and the generally small excitation cross sections. Nevertheless, nitrogen was preferably detected in MP-SiBPy, MP-SiBPy-Co, and MP-SiBPy-Co-PPz4, as expected from bipyridine moieties as well as poly(organo)phosphazene PPz4. Copper appears across all spectra due to scattered radiation exciting X-rays in the copper mesh grid. A significant sulfur peak was only found for MP-SiBPy-Co-PPz4, which suggests that only the sulfur from the PPz4 was detected, as the sulfur signal is accompanied by a phosphorus peak.

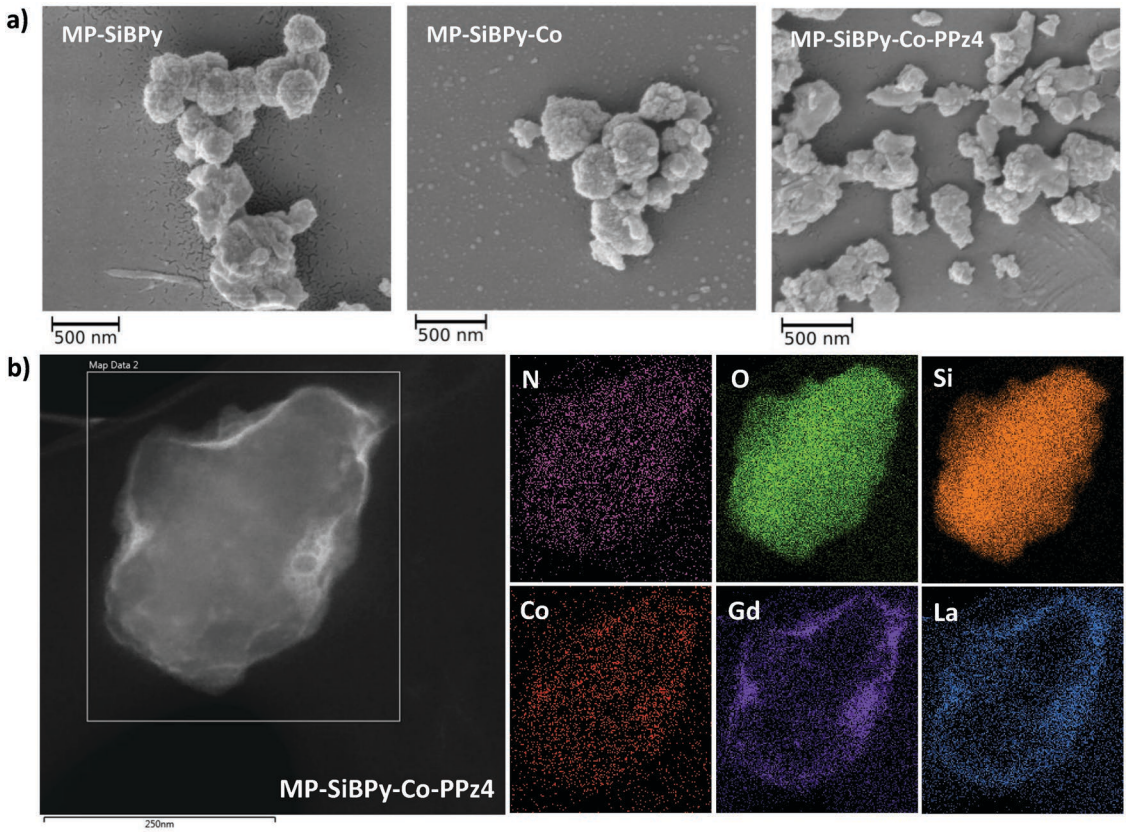

Figure 3. a) SEM InLens images taken with 3 keV beam energy: microparticles were dispersed on a flat silicon wafer and sputter coated with gold (10 nm), observing individual amorphous microparticles forming aggregates. Scale bar: 500 nm. b) STEM-EDX mapping of amorphous MP-SiBPy-Co-PPz4 particle stained with UranyLess (uranium-free staining contrast solution). La and Gd elements highly stained the organic parts of the system (a significantly coverage of the PPz4 on the surface of the silica particles was demonstrated). Scale bar: 250 nm.

Apparently, the small sulfur content in bipyridine could not be reliably detected.

In order to visualize the grafted polymer on the surface of the silica, the material MP-SiBPy-Co-PPz4 was stained and measured by STEM-EDX mapping measurements. A significant coverage of the stained polymer was detected (Figure 3b) mainly on the surface of the amorphous silica-based microparticles (since only the organic coverage was stained with contrast stain solution of non-radioactive lanthanides), and therefore, confirming the well-performed functionalization step. Additionally, the zeta potentials were measured (Table 1, Figure S9d, Supporting Information) to determine the surface properties of all four materials. The surface of bare MP-nf (containing 100% TEOS) is commonly highly negative due to the presence of free charged −OH groups (−42.8 mV). Similarly, the MP-SiBPy showed a negative charge (−41.9 mV) which indicated that the surface was not significantly affected by the 5% of ligands content against 95% TEOS. Interestingly, the surface modification with the polymer PPz4 exhibited a positive increase of the charge (−28.6 mV in final MP-SiBPy-Co-PPz4) which suggested an effective polymer grafting step by chemical Si−O−Si bonding formation.

The evaluation of the polymeric switch on the micromotor MP-SiBPy-Co-PPz4 was carried out and the accessibility of the fuel (hydrogen peroxide) to the metal center from the MP-SiBPy-Co was investigated. To this end, aqueous suspensions of cobalt containing microparticles (MP-SiBPy) were placed on an optical microscope glass slide and images and videos were recorded (**Figure 4**a and see recorded video SV1, Supporting Information). The system MP-SiBPy-Co was mixed with water and, as expected, no oxygen production was observed (Figure 4a). When the same experiment was performed with hydrogen peroxide (15 vol%) using MP-SiBPy-Co, oxygen bubbles were clearly formed and ejected from the microparticles to the upper site of the aqueous drop containing fuel (Figure 4b). This was attributed to the catalytic decomposition of hydrogen peroxide in water and oxygen gas from the metal catalyst located in the mesopores. To obtain homogeneous bubble growth, the need of a tube-like structural design was reported to enhance the oxygen production in micro/nanotubes.[37] A high-aspect of our selected type of silica materials is the vast number of cylindrical and homogeneous longitudinal mesopores present per particle. Thus, we could assume that this effect may also appear in our proposed system and possibly boost a better bubble growth and ejection control from the inner to the outer pores. Our results clearly demonstrate the potential behavior of the designed micromotor based on mesoporous silica particles. However, it is worth mentioning that the amorphous morphology of the microparticles prepared here and their tendency to aggregate (as was already shown in SEM images, Figure 2c),

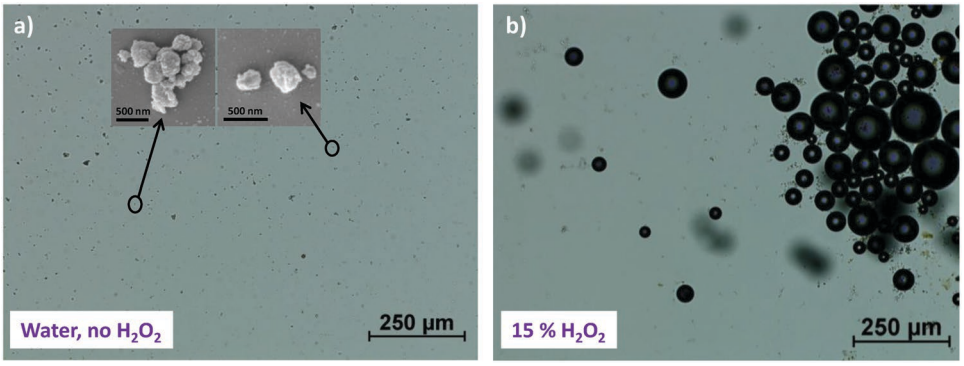

Figure 4. a) Optical microscope images of the cobalt containing microparticles functionalized with bipyridine (MP-SiBPy-Co) in water, observing no bubbles formation. Inset a) SEM InLens images taken with 3 keV beam energy of MP-SiBPy-Co microparticles dispersed on a flat silicon wafer and sputter coated with gold (10 nm), where individual microparticles (≤500 nm in diameter) are visible (left) and micromotor aggregations (right), scale bar = 500 nm. b) In 15 vol% H_2O_2 (fuel), the O_2 bubbles are formed immediately. Scale bar: 250 µm.

made challenging to observe any motion in general, and hence, any directionality or even motion (see recorded video SV3, Supporting Information).

After confirming the catalytic capability of the cobalt-containing mesoporous microparticles (MP-SiBPy-Co), the function of the polymeric switches attached onto the micromotors (MP-SiBPy-Co-PPz4) was tested. For that, both non-polymer coated particles MP-SiBPy-Co and polymer coated MP-SiBPy-Co-PPz4 particles were heated up from 15 to 35 °C. Satisfactory, the temperature-dependent behavior of our design micromotor was recorded (see video SV1, Supporting Information) and clearly demonstrated. When no polymer was present, a continued oxygen evolution with no changes at increasing temperatures was observed. However, when the polymer PPz4 was present, the material did not respond upon temperatures below 25 °C. In fact, this temperature-regulatory system was designed to facilitate a switching off–on bubble formation on demand by simply heating the particles mildly. A possible roughness surface due to the polymer coating may result in the reduction of bubble formation. Nevertheless, the vast number of non-connected and tube-like mesoporous allows individual blocking and more controlled coating of the surface. These features highlight the use of mesoporous silica microparticles in the design of advanced micromotors, among other materials. It should be noted that the grafting of the polymer apparently affects the accessibility of catalytic centers, where the non-coated particles showed a significant higher activity under analogous conditions than the polymer-functionalized particles (see videos in the Supporting Information).

The reversibility of the polymer was positively confirmed by several cooling–heating cycles, after demonstrating the potential external thermoresponsive control of our micromotors. In the following images, the microparticles are shown at different temperatures during a previous adjusted temperature-program, changing from 15 to 30 °C and vice versa (**Figure 5**a). The bubble evolution was recorded initially from 15 to 20 °C where no bubbles were observed since the polymer was in swollen state, blocking the pores and causing complete diffusion

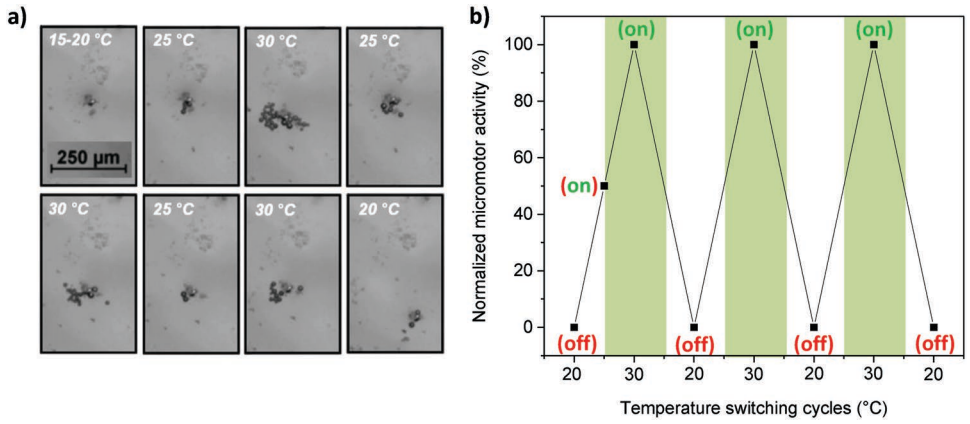

Figure 5. a) Optical microscope images captured from MK-SiBPy-Co-PPz4 microparticles covered with the thermoresponsive-derived polyphosphazene at different temperatures (at 15 °C min^{-1} as heating rate with 15 vol% H_2O_2) showing the reversibility of the system by heating up from 15 to 20 °C (off), 25 °C (starting-on switch), 30 °C (on), cooling down to 25 °C (still on mode), heating up to 30 °C (on) and cooling down to 25 °C (on mode), then heating up to 30 °C (on) and cooling down back to 20 °C (begging to stop). b) Schematic qualitative representation of three complete heating–cooling cycles from 20 to 30 °C which shows the repeatable and reproducible off–on switch owned by the reversible LCST behavior of PPz4 brushes.

hindrance of the hydrogen peroxide into the pores or the surface of the micromotors (switched "off" state). At 25 °C, few oxygen bubbles started forming whereas at 30 °C, the highest bubble formation was obtained. This behavior was in agreement to the expected collapsing of the polymer brushes (see scheme in Figure 1) located on the silica surface and exposing the cobalt located in the pores to the fuel. These promising results showed the clear temperature off–on switching mechanism effect of the polymer on the accessibility of the H_2O_2 to the cobalt (see in live reversible behavior in Video SV2, Supporting Information). The potential thermoresponsive reversibility of the system was still observed after at least three "on–off" cycles due to the reversible LCST behavior of polymer PPz4 (Figure 5b) assuming a temperature controlled repeatable and reproducible.

Oxygen evolution from silica mesoporous microparticles containing bipyridine-cobalt ligands could be reversibly controlled on demand via surface grafting of silane-derived thermosensitive polymer. For the development of the on–off switch, a poly(organo)phosphazene was synthesized and derived with thermoresponsive Jeffamine M-2005 and alkyl chains to add thermoresponsive behavior and with alkoxysilanes groups to enable the surface grafting to the silica surface. During measurements under an optical microscope, the evolution of oxygen from temperatures above 25 °C was clearly detected by the formation of gas bubbles in presence of the fuel, hydrogen peroxide in 15 vol% concentrations. Below this temperature, no bubbles were observed, indicating that the system could be switched off at-will within a mild drop in temperature. Furthermore, the reversible switch mechanism was verified by at least three repeated heating–cooling cycles from 20 to 30 °C (supported videos and images) demonstrating the repeatable and reproducible thermoresponsive polymeric switch. The temperature transition of the polymer could be easily modified in future work by changing the substituents ratio from the polyphosphazene backbone. The use of mesoporous silica particles to build micromotors may be a potential support candidate to enhance the bubbles growth and further propulsion due to their unique longitudinal and homogeneous porosity distribution. The performance of these micromotors could be further improved to enable directional motion and could then be easily adapted to a wide range of applications that require external control, such as environmental treatment or medicine, targeting, for example, biologically relevant temperatures.

Supporting Information

Supporting Information is available from the Wiley Online Library or from the author.

Acknowledgements

The authors acknowledge Prof. O. Brüggemann for the access to laboratory resources and M.K. acknowledges the Johannes Kepler University for financial support. The authors gratefully acknowledge the collaboration and support of Prof. N. S. Sariciftci within his Wittgenstein Prize Project from Austrian Science Foundation (FWF Z-222 N19). T.T. and H.G. also gratefully acknowledge the financial support by the Austrian Federal Ministry for Digital and Economic Affairs and the National Foundation for Research, Technology and Development in the frame of the CDL for Nanoscale Phase Transformations. NMR experiments were performed at the Upper Austrian–South Bohemian Research Infrastructure Center in Linz, co-financed by "RERI-uasb", EFRE RU2-EU-124/100-2010 (ETC Austria–Czech Republic 2007–2013, Project M00146). The authors acknowledge the Linz Institute of Technology, Johannes Kepler University at Linz, and the State of Upper Austria (Project LIT 213760001 DEG-PMO) for the fundings.

Conflict of Interest

The authors declare no conflict of interest.

Keywords

mesoporous silica particles, micromotors, oxygen evolution, polyphosphazenes, thermoresponsive molecular gates

Received: July 10, 2019
Revised: September 19, 2019
Published online: October 21, 2019

[1] a) V. Garcia-Gradilla, J. Orozco, S. Sattayasamitsathit, F. Soto, F. Kuralay, A. Pourazary, A. Katzenberg, W. Gao, Y. Shen, J. Wang, *ACS Nano* **2013**, *7*, 9232; b) M. Ibele, T. E. Mallouk, A. Sen, *Angew. Chem., Int. Ed.* **2009**, *48*, 3308; c) Y. Hong, M. Diaz, U. M. Córdova-Figueroa, A. Sen, *Adv. Funct. Mater.* **2010**, *20*, 1568.
[2] a) S. Sanchez, A. A. Solovev, Y. Mei, O. G. Schmidt, *J. Am. Chem. Soc.* **2010**, *132*, 13144; b) W. Gao, A. Pei, J. Wang, *ACS Nano* **2012**, *6*, 8432; c) W. Gao, A. Uygun, J. Wang, *J. Am. Chem. Soc.* **2012**, *134*, 897.
[3] a) S. Balasubramanian, D. Kagan, K. M. Manseh, P. Calvo-Marzal, G. U. Flechsig, J. Wang, *Small* **2009**, *5*, 1569; b) X. Ma, X. Wang, K. Hahn, S. Sánchez, *ACS Nano* **2016**, *10*, 3597.
[4] V. Magdanz, G. Stoychev, L. Ionov, S. Sanchez, O. Schmidt, *Angew. Chem., Int. Ed.* **2014**, *53*, 2673.
[5] a) Q. Fu, G. V. Rama Rao, T. L. Ward, Y. Lu, G. P. Lopez, *Langmuir* **2007**, *23*, 170; b) Q. Fu, G. V. Rama Rao, L. K. Ista, Y. Wu, B. P. Andrzejewski, L. A. Sklar, T. L. Ward, G. P. López, *Adv. Mater.* **2003**, *15*, 1262.
[6] M. Mas, I. Galiana, S. Hurtado, L. Mondragón, A. Bernardos, F. Sancenón, M. D. Marcos, P. Amorós, N. Abril-Utrillas, R. Martínez-Máñez, J. R. Murguía, *Int. J. Nanomed.* **2014**, *9*, 2597.
[7] P. Nadrah, F. Porta, O. Planinsek, A. Kros, M. Gaberscek, *Phys. Chem. Chem. Phys.* **2013**, *15*, 10740.
[8] Q. Xing, N. Li, D. Chen, W. Sha, Y. Jiao, X. Qi, Q. Xu, J. Lu, *J. Mater. Chem. B* **2014**, *2*, 1182.
[9] E. Climent, L. Mondragón, R. Martínez-Máñez, F. Sancenón, M. D. Marcos, J. R. Murguia, P. Amorós, K. Rurack, E. Pérez-Payá, *Angew. Chem., Int. Ed.* **2013**, *52*, 8938.
[10] a) F. Li, Y. Zhu, Y. Wang, *Microporous Mesoporous Mater.* **2014**, *200*, 46; b) F. Mou, C. Chen, Q. Zhong, Y. Yin, H. Ma, J. Guan, *ACS Appl. Mater. Interfaces* **2014**, *6*, 9897; c) J. Kobayashi, T. Okano, *Bull. Chem. Soc. Jpn.* **2019**, *92*, 817.
[11] Q. Zhang, G. Vancoillie, M. A. Mees, R. Hoogenboom, *Polym. Chem.* **2015**, *6*, 2396.
[12] F. Hapiot, S. Menuel, E. Monflier, *ACS Catal.* **2013**, *3*, 1006.
[13] Y. Tu, F. Peng, X. Sui, Y. Men, P. B. White, J. C. M. van Hest, D. A. Wilson, *Nat. Chem.* **2017**, *9*, 480.
[14] H. G. Schild, *Prog. Polym. Sci.* **1992**, *17*, 163.
[15] S. Rothemund, I. Teasdale, *Chem. Soc. Rev.* **2016**, *45*, 5200.

[16] I. Teasdale, *Eur. J. Inorg. Chem.* **2019**, *2019*, 1445.
[17] J. X. Zhang, L. Y. Qiu, K. L. Zhu, Y. Jin, *Macromol. Rapid Commun.* **2004**, *25*, 1563.
[18] G. D. Kang, S. H. Cheon, S.-C. Song, *Int. J. Pharm.* **2006**, *319*, 29.
[19] S. Wilfert, A. Iturmendi, Henke, O. Brüggemann, I. Teasdale, *Macromol. Symp.*, **2014**, *337*, 116.
[20] J. Li, X. Yu, M. Xu, W. Liu, E. Sandraz, H. Lan, J. Wang, S. M. Cohen, *J. Am. Chem. Soc.* **2017**, *139*, 611.
[21] a) D. Brunel, *Microporous Mesoporous Mater.* **1999**, *27*, 329; b) C. T. Kresge, M. E. Leonowicz, W. J. Roth, J. C. Vartuli, J. S. Beck, *Nature* **1992**, *359*, 710.
[22] a) X. Ma, A. Jannasch, U.-R. Albrecht, K. Hahn, A. Miguel-López, E. Schäffer, S. Sánchez, *Nano Lett.* **2015**, *15*, 7043; b) A. C. Hortelão, T. Patiño, A. Perez-Jiménez, À. Blanco, S. Sánchez, *Adv. Funct. Mater.* **2018**, *28*, 1705086; c) J. Shao, M. Xuan, H. Zhang, X. Lin, Z. Wu, Q. He, *Angew. Chem., Int. Ed.* **2017**, *56*, 12935.
[23] F. Sancenón, L. Pascual, M. Oroval, E. Aznar, R. Martínez-Máñez, *Chem. Open* **2015**, *4*, 418.
[24] a) A. P. Wight, M. E. Davis, *Chem. Rev.* **2002**, *102*, 3589; b) S. Huh, J. W. Wiench, J.-C. Yoo, M. Pruski, V. S.-Y. Lin, *Chem. Mater.* **2003**, *15*, 4247.
[25] P. Van Der Voort, D. Esquivel, E. De Canck, F. Goethals, I. Van Driessche, F. J. Romero-Salguero, *Chem. Soc. Rev.* **2013**, *42*, 3913.
[26] a) M. P. Kapoor, Q. Yang, S. Inagaki, *J. Am. Chem. Soc.* **2002**, *124*, 15176; b) W. R. Grüning, G. Siddiqi, O. V. Safonova, C. Copéret, *Adv. Synth. Catal.* **2014**, *356*, 673.
[27] W. F. Paxton, A. Sen, T. E. Mallouk, *Chem. Eur. J.* **2005**, *11*, 6462.
[28] J. J. Teesdale, A. J. Pistner, G. P. A. Yap, Y.-Z. Ma, D. A. Lutterman, J. Rosenthal, *Catal. Today* **2014**, *225*, 149.
[29] a) S.-P. Luo, L.-Z. Tang, S.-Z. Zhan, *Inorg. Chem. Commun.* **2017**, *86*, 276; b) R. A. Heckman, J. H. Espenson, *Inorg. Chem.* **1979**, *18*, 38.
[30] A. Linhardt, M. König, A. Iturmendi, H. Henke, O. Brüggemann, I. Teasdale, *Ind. Eng. Chem. Res.* **2018**, *57*, 3602.
[31] K. Sarkar, Y. Salinas, I. Campos, R. Martínez-Máñez, M. D. Marcos, F. Sancenón, P. Amorós, *ChemPlusChem* **2013**, *78*, 684.
[32] Y. Salinas, M. V. Solano, R. E. Sørensen, K. R. Larsen, J. Lycoops, J. O. Jeppesen, R. Martínez-Máñez, F. Sancenón, M. D. Marcos, P. Amorós, C. Guillem, *Chem. Eur. J.* **2014**, *20*, 855.
[33] V. Muriel-Galet, E. Pérez-Esteve, M. Ruiz-Rico, R. Martínez-Máñez, J. M. Barat, P. Hernández-Muñoz, R. Gavara, *Nanomaterials* **2018**, *8*, 865.
[34] C. D. Nunes, A. A. Valente, M. Pillinger, A. C. Fernandes, C. C. Romão, J. Rochaa, I. S. Gonçalves, *J. Mater. Chem.* **2002**, *12*, 1735.
[35] H. Takeda, M. Ohashi, T. Tani, O. Ishitani, S. Inagaki, *Inorg. Chem.* **2010**, *49*, 4554.
[36] H. Henke, O. Brüggemann, I. Teasdale, *Macromol. Rapid Commun.* **2017**, *38*, 1600644.
[37] Y. Salinas, A. Agostini, E. Pérez-Esteve, R. Martínez-Máñez, F. Sancenón, M. D. Marcos, J. Soto, A. M. Costero, S. Gil, M. Parra, P. Amorós, *J. Mater. Chem. A* **2013**, *1*, 3561.